Dynamics and structure of nickel chloride–methanol solutions: quasi-elastic neutron scattering and molecular dynamics simulations

2007 J. Phys.: Condens. Matter 19 415120

(http://iopscience.iop.org/0953-8984/19/41/415120)

IOP PUBLISHING JOURNAL OF PHYSICS: CONDENSED MATTER

J. Phys.: Condens. Matter **19** (2007) 415120 (22pp) doi:10.1088/0953-8984/19/41/415120

Dynamics and structure of nickel chloride–methanol solutions: quasi-elastic neutron scattering and molecular dynamics simulations

Ashok K Adya[1,4], **Oleg N Kalugin**[2] **and W Spencer Howells**[3]

[1] Condensed Matter Group and BIONTHE[5] Centre, School of Contemporary Sciences, University of Abertay Dundee, Bell Street, Dundee DD1 1HG, UK
[2] Department of Inorganic Chemistry, Kharkiv National University, Svobody square 4, Kharkiv 61077, Ukraine
[3] ISIS, Rutherford Appleton Laboratory, Chilton, Didcot, Oxon OX11 0QX, UK

E-mail: A.K.Adya@abertay.ac.uk, Oleg.N.Kalugin@univer.kharkov.ua and w.s.howells@rl.ac.uk

Received 30 April 2007, in final form 2 July 2007
Published 27 September 2007
Online at stacks.iop.org/JPhysCM/19/415120

Abstract

The high-resolution quasi-elastic neutron scattering (QENS) technique has been applied to study the translational diffusion of methanol protons in pure methanol (MeOH) at 223 and 297 K, and in 0.3 and 1.3 molal non-aqueous electrolyte solutions (NAESs) of $NiCl_2$ in methanol at 297 K. Molecular dynamics (MD) simulations, in conjunction with the present QENS results and our previously published structural results obtained by neutron diffraction isotopic substitution (NDIS) experiments, have been carried out in the NVT ensemble to explore the particle dynamics and microscopic structures of the experimentally investigated systems. The simulated structure of the ∼1.35 molal $NiCl_2$–MeOH NAES has been compared with the structures of Ni^{2+} and Cl^- coordination shells in ∼1.4 molal NAES obtained earlier by the NDIS technique.

1. Introduction

Our ability to understand and predict the properties of disordered materials continues to be a challenge for condensed matter theory. Within this area the non-aqueous electrolyte solutions (NAESs) perhaps remain the severest test. Ion solvation and ion association are the two phenomena which mainly govern the macroscopic properties of NAESs and, hence, their technological applications. A deeper understanding of these phenomena requires detailed information of ion–solvent and ion–ion interactions at a molecular level.

[4] Author to whom any correspondence should be addressed.
[5] BIO- and Nano-Technologies for Health and Environment.

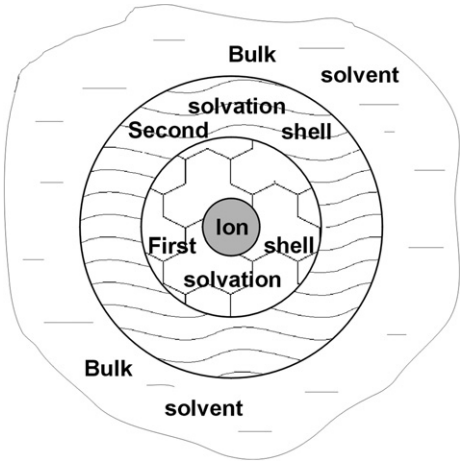

Figure 1. Model of ion solvation in solution with the three regions of a solvent defined according to Frank and Wen [1] as the first solvation shell (FSS), second solvation shell (SSS), and bulk solvent (Bulk).

The solvation of ions in a liquid solvent embodies primarily the interactions between the ions and solvent molecules that alter the solvent structure and its microdynamics in solution. According to the Frank and Wen model of ion solvation [1] the space around an ion can be divided into three regions, namely the first solvation shell (FSS), second solvation shell (SSS), and bulk solvent (see figure 1). In the bulk solvent its properties correspond to those in neat solvent. In the FSS the solvent properties are modified significantly by an ion, while the SSS is the intermediate region between the bulk solvent and the FSS. It is now entirely clear that the problems associated with the interactions of various types in solution, the structure of the solution, and the thermal movement of its particles are intimately related to each other.

Among the various direct experimental methods (i.e., those methods for which the space and time dimensions are comparable to the molecular dimensions and characteristic times of molecular processes, respectively), neutron diffraction with isotopic substitution (NDIS) [2–6] and quasi-elastic neutron scattering (QENS) [7–11] offer the most powerful techniques for analysing the microscopic structure and ion/molecule dynamics in ion–molecular systems. These methods allow us to derive structural information of the nearest-neighbour ion environment in terms of pair radial distribution functions, interatomic distances and co-ordination numbers, and molecular dynamics in terms of the dynamic structure factors and diffusion coefficients.

When these neutron scattering techniques are complementarily coupled with modern molecular modelling techniques, such as molecular dynamics (MD) computer simulations, the output can provide structural and dynamical details of unparalleled accuracy not obtainable by the application of any single technique [12, 13].

Recently, we demonstrated [14, 15] the use of the NDIS technique to isolate the ion–ion, ion–H and ion–O partial radial distribution functions (RDFs), and to resolve the co-ordination/solvation structures of the isotopically substituted ions (cation and anion) in $NiCl_2$–MeOH solutions. First- , second- and higher-order difference methods of neutron diffraction with isotopic substitutions on nickel, chlorine and hydroxyl hydrogen (H_O) were applied in conjunction with *ab initio* calculations of the Ni^{2+}–methanol complex to derive Ni–O, Ni–H_O, Ni–Cl, Ni–C, Ni–H (methyl), and Cl^--dependent pair RDFs. Analyses of these RDFs

demonstrated, in most clear terms, that Ni^{2+} is co-ordinated octahedrally by five methanol molecules and one chloride anion. The solvation number of Cl^- was determined to be $\cong 2$. The joint analysis of the pair RDFs, $g_{NiCl}(r)$ and $g_{ClCl}(r)$, revealed that the electrolyte in its 1.4 molal methanolic solution mainly exists in the form of solvated contact ion pairs, $[NiCl]_s^+$, with a very small content of solvated $[NiCl_2]_s^0$ ion triples.

From this point of view there is special interest in the study of dynamic aspects of ion solvation phenomena in $NiCl_2$–methanol solutions by using the quasi-elastic neutron scattering technique and molecular dynamics simulations.

In their seminal paper, Hewish *et al* [7] showed how the technique of QENS at high (μeV) resolution could be used to probe, via the dynamic structure factor, $S(k, \omega)$, the dynamics of protons in hydrogenous liquids. Using the model of Frank and Wen, they were able to analyse the spectroscopic information derived from QENS in terms of the lifetimes of water molecules in the cationic hydration structures and water diffusion coefficients, and thereby obtain complementary information to that obtained from the nuclear magnetic relaxation method and other spectroscopic techniques. Analyses of QENS results, although slightly model dependent, require surprisingly few assumptions and can give a definitive picture of the dynamics of protons of the solvent molecules, especially with regard to how the first solvation shell of the ion develops as the ionic concentration and temperature are varied.

The work presented in this paper aims to use a state-of-the-art approach of jointly applying the three techniques, namely NDIS, QENS and MD simulations, for detailed investigation of the structural and dynamic properties of neat methanol (MeOH) and $NiCl_2$–MeOH solutions at different temperatures and salt concentrations.

The paper has the following structure. The experimental method is given in section 2. Section 3 describes the essential theory behind the QENS method, data analyses, and discussion of the results. The details of MD simulations are described in section 4 with special attention paid to the validation of the force field model employed and comparison with the NDIS results. In section 5, the results of MD simulations are presented and discussed.

2. Experimental details

The aqueous solutions of $NiCl_2$ were obtained by dissolving crystalline $NiCl_2{\cdot}xH_2O$ (Alfa, Puratronic®, 99.995%) in very dilute HCl (BDH, Aristar®) solution to remove any residual products of hydrolysis. The solutions of $NiCl_2$ were then evaporated to a solid form of $NiCl_2{\cdot}6H_2O$ and further dried in a vacuum line under 1–100 Pa at gradually increasing temperatures from 25 to 70 °C during a period of one month. Such a procedure reduced the water content to less than 0.01%, which was controlled/monitored by weighing with corresponding accuracy. The anhydrous salt, as expected [16], was a yellow-brownish powder.

The solutions of $NiCl_2$ in methanol (Analar, 99.8%, <0.001% H_2O) of required concentrations were made by weighing in a dried nitrogen-filled glove box. Prior to this, however, the solvent was distilled and dried under 4 Å molecular sieves for one week.

The sample densities were measured by using an Anton Paar DMA 58 densimeter.

The quasi-elastic neutron scattering experiments were performed on the backscattering spectrometer IN10 at the ILL, Grenoble, France. Spectra were measured at five equally spaced k-values in the range $0.09\ \text{Å}^{-1} \leqslant k \leqslant 0.38\ \text{Å}^{-1}$ with an energy window of about $\pm 15\ \mu$eV. Incident wavelength of 6.271 Å with the resolution in momentum transfer of $0.04\ \text{Å}^{-1}$ was used. The monochromator was standard Si(111) and the experimental energy resolution function of $\approx 1.5\ \mu$eV (HWHM) was obtained from incoherent scattering from a sample of vanadium.

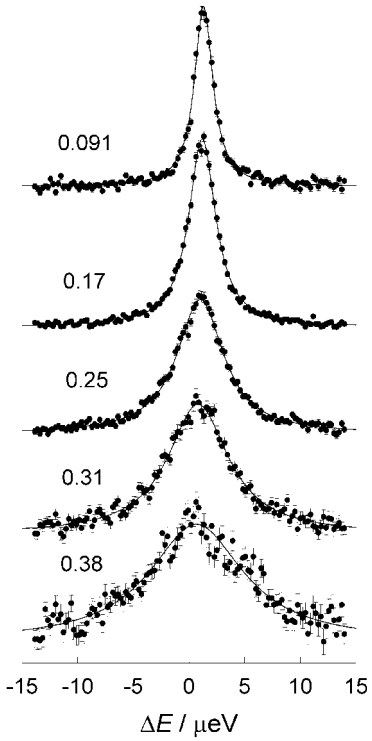

Figure 2. The experimental quasi-elastic neutron spectra (points) and fitted Lorentzians (solid lines) for neat methanol (MeOH) at 223 K at five different k-values (0.091, 0.17, 0.25, 0.31, and 0.38) in Å^{-1} indicated in the figure, with arbitrary scale on the ordinate.

The complete experiment required measurements to be taken of the liquid sample (methanol or $NiCl_2$ solutions in methanol) in its container, the empty container, the background, and a vanadium slab of 1 mm thickness to give the energy resolution function.

The samples were held in a 40 mm × 40 mm flat container specially made from PTFE material with a sample thickness of 1 mm, providing a sample volume of 1.6 cm^3. All the measurements were performed at two temperatures, 223±1 K and ambient (nominal 297±1 K).

The raw data were converted to the dynamic structure factors, $S(k, \omega)$, and corrected for background and container scattering using the INX program at the ILL. No multiple scattering corrections were applied to the data. The experimental QENS spectra on neat methanol and 0.3 and 1.3 molal $NiCl_2$–MeOH solutions are shown in figures 2–5.

3. QENS data analyses and discussion of the results

The scattering of neutrons from a solution comprising n atomic species is dependent on the double differential cross section $\frac{d^2\sigma}{d\Omega\, d\omega}$ defined by [7, 9]

$$\frac{d^2\sigma}{d\Omega\, d\omega} = \sum_i^n \sum_j^n b_i b_j (x_i x_j)^{1/2} S_{ij}(k, \omega) + \sum_i^n b_{\text{inc},i}^2 x_i S_i^s(k, \omega), \tag{1}$$

where x_i, b_i and $b_{\text{inc},i}$ are the atomic fraction, coherent scattering length and incoherent scattering length of species i, $S_i^s(k, \omega)$ is the self-part of the scattering law, and $\hbar k = \Delta p$

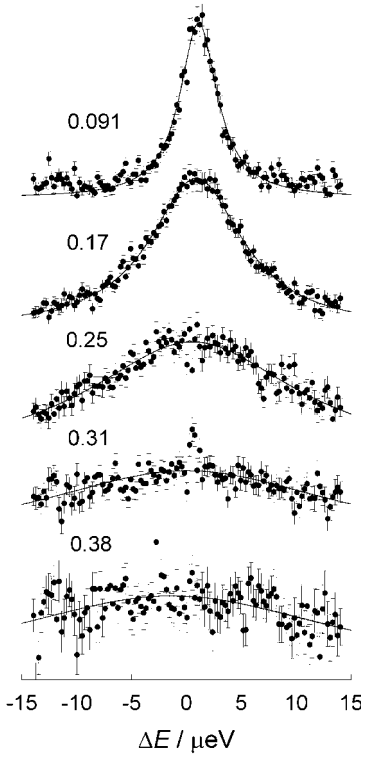

Figure 3. The experimental QENS spectra (points) and fitted Lorentzians (solid lines) for neat methanol at 297 K at five different k-values in Å^{-1} indicated in the figure, with arbitrary scale on the ordinate.

and $\hbar\omega = \Delta E$ are the momentum and energy transfers, respectively. The incoherent scattering cross section of the hydrogen (H) nucleus present in all the non-aqueous solvents, including methanol, is so large that $S(k, \omega)$ is dominated by the self-term, $S_{\mathrm{H}}^{\mathrm{s}}(k, \omega)$; the other terms are sufficiently small that they may be neglected in the data analysis. The knowledge of $\frac{\mathrm{d}^2\sigma}{\mathrm{d}\Omega\,\mathrm{d}\omega}$ should, thus, lead directly to the proton dynamics, which can be identified with that of the solvent molecule itself.

For a proton obeying the diffusion equation, $S_{\mathrm{H}}^{\mathrm{s}}(k, \omega)$ is a Lorentzian of the form

$$S_{\mathrm{H}}^{\mathrm{s}}(k, \omega) = (1/\hbar)Dk^2 \big/ \left[(Dk^2)^2 + \omega^2\right], \tag{2}$$

with translational diffusion coefficient, D. This is the form to be expected when the longest ionic binding time, τ_{b}, present is short relative to the observation time, τ_{ob}, so that during this observation time any proton can sample the entire range of environments present in the solution. Usually this situation is described as the 'fast-exchange limit' [7].

For the case when the solvent molecule's binding time (usually to a cation) is longer than the observation time, i.e., when $\tau_{\mathrm{b}} > \tau_{\mathrm{ob}}$, the so-called 'slow-exchange regime', $S_{\mathrm{H}}^{\mathrm{s}}(k, \omega)$ takes the form

$$S_{\mathrm{H}}^{\mathrm{s}}(k, \omega) = (1/\hbar)\left\{x_1 D_1 k^2 \big/ \left[(D_1 k^2)^2 + \omega^2\right] + x_2 D_2 k^2 \big/ \left[(D_2 k^2)^2 + \omega^2\right]\right\}, \tag{3}$$

which is a sum of two weighted Lorentzians with two different diffusion coefficients, D_1 and D_2 in the FSS and SSS (or bulk solvent), respectively. Here x_i $(i = 1, 2)$ denote the atomic fractions of the two proton populations.

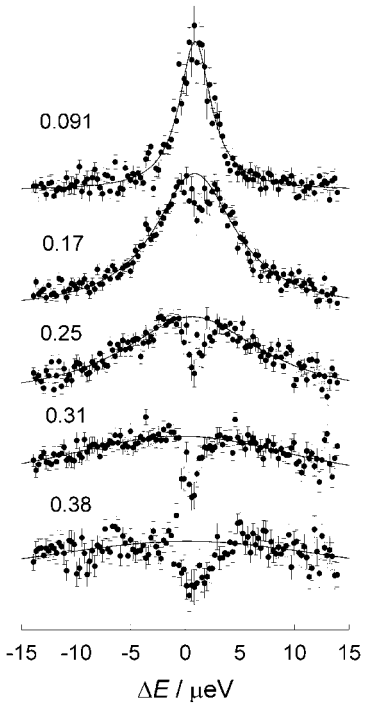

Figure 4. The experimental QENS spectra (points) and fitted Lorentzians (solid lines) for 0.3 molal solution of $NiCl_2$ in methanol at 297 K at five different k-values in $Å^{-1}$ indicated in the figure, with arbitrary scale on the ordinate.

Bearing in mind the results of aqueous $NiCl_2$ solutions [7], one can expect the methanolic solutions of this salt also to obey the 'slow-exchange regime'. Accordingly, the two separate translational diffusion coefficients of MeOH molecules, one originating from the Ni^{2+} FSS and the other from the rest of the solution, can, in principle, be evaluated. But, due to the relatively high statistical noise observed, especially at ambient temperature (figures 3–5), and the narrow energy window available, the fitting procedure did not allow us to resolve more than a single Lorentzian (see the solid lines in figures 2–5). The experimental neutron spectra of $NiCl_2$ solutions could thus be described by a scattering law in the form

$$S(k,\omega) = (1/\hbar)\bar{D}k^2/\left[(\bar{D}k^2)^2 + \omega^2\right], \tag{4}$$

where

$$\bar{D} = x_1 D_1 + x_2 D_2, \tag{5}$$

is the average translational diffusion coefficient of MeOH molecules throughout the whole solution. Clearly, the experimental spectra for neat methanol at both the temperatures were fitted by a single Lorentzian each in the form of equation (2). Then, the slopes of the plots of the half-width at half-maximum (HWHM) of the fitted Lorentzians versus the square of wavenumber (k^2 in $Å^{-2}$) were used to calculate the corresponding diffusion coefficients (figure 6). It should be noted, however, that for the 0.3 molal $NiCl_2$–MeOH solutions, only the first four points, respectively, could be used because of large statistical errors in HWHM values at high k-values. The experimental diffusion coefficients, D (for neat methanol) and $\bar{D}$ (for $NiCl_2$–MeOH solutions) are listed in table 1 along with the available literature [11, 17, 18] data

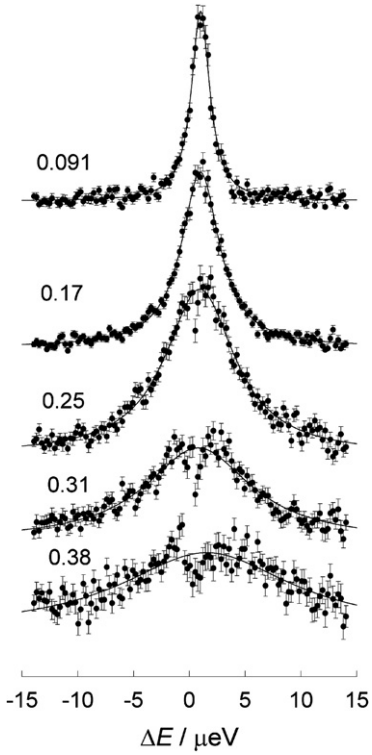

Figure 5. The experimental QENS spectra (points) and fitted Lorentzians (solid lines) for 1.3 molal solution of $NiCl_2$ in methanol at 297 K at five different k-values in $Å^{-1}$ indicated in the figure, with arbitrary scale on the ordinate.

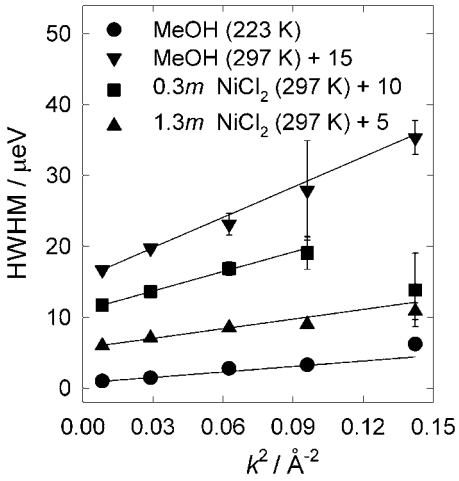

Figure 6. The half-widths at half-maxima (HWHM) of the fitted Lorentzians plotted as a function of the square of wavenumber (k^2 in $Å^{-2}$) for neat methanol at 223 and 297 K, and for 0.3 and 1.3 molal $NiCl_2$ solutions in methanol at 297 K.

on neat methanol. The analysis of table 1 firstly shows that the D values for neat methanol agree well with the literature data. Secondly, as the temperature decreases and concentration of $NiCl_2$

Table 1. The diffusion coefficients of methanol (MeOH) in neat solvent and $NiCl_2$–MeOH systems.

System	Temperature, T (K)	$\Delta E/k^2$ [a] (μeV Å^2)	Diffusion coefficient of MeOH[f], D (10^9 m^2 s^{-1})
CH_3OH (MeOH)	223	20.8 ± 2.2	0.39 ± 0.03[b], 0.498[c]
CH_3OH (MeOH)	297	142 ± 4	2.16 ± 0.07[b], 2.567[c], 2.50[d], 3.25[e]
0.3 molal $NiCl_2$ in MeOH	297	92.0 ± 3.0	1.40 ± 0.05[b]
1.3 molal $NiCl_2$ in MeOH	297	45.3 ± 4.6	0.69 ± 0.07[b]

[a] Gradient of a plot of HWHM $\Delta E(\mu\text{eV})$ versus k^2 (Å^{-2}), see figure 6.
[b] Present work.
[c] Reference [11] (data refer to CD_3OH at 300 and 230 K).
[d] Reference [17].
[e] Reference [18].
[f] For the $NiCl_2$–MeOH solutions, this value corresponds to the average diffusion coefficient, $\bar{D}$, defined in equation (5).

Table 2. Some parameters of the modelled systems and MD simulation details. (Note: the sign $\Rightarrow$ means approaching.)

Designation of the system	Solute[a]	Number of MeOH molecules	Molality, m (mol kg^{-1})	Temperature, T (K)	Density, ρ (g cm^{-3})	Dielectric constant[b]
I	—	216	0	223	0.857 11	52.32
II	—	216	0	298.15	0.786 37	32.66
III	1 Ni^{2+}	215	$\Rightarrow$0	298.15	0.786 37	32.66
IV	1 Cl^-	215	$\Rightarrow$0	298.15	0.786 37	32.66
V	2 $NiCl_2$	210	$\approx$0.3	298.15	0. 8229	32.66
VI	9 $NiCl_2$	189	$\approx$1.35	298.15	0. 9592	32.66

[a] The number before each solute refers to the number of ions or number of molecules of the electrolyte.
[b] The values used for calculation of Coulombic interactions by reaction field method.

increases, the diffusion of MeOH molecules slows down drastically. Unfortunately, as our results show, the QENS technique does not on its own allow one to elucidate any microscopic details of solvent dynamics in the cation's solvation shell. The MD simulations were, therefore, used complementarily in this work to elucidate all the details of ion solvation dynamics.

4. MD simulation details

The MD simulations of pure MeOH at 223 and 298.15 K (systems I and II), infinitely dilute solutions of Ni^{2+} and Cl^- (systems III and IV), and solutions of $NiCl_2$ in MeOH of different concentrations (systems V and VI) were performed in a cubic box with periodic boundary conditions. The box lengths for the systems I–IV and V–VI were chosen to match the experimental densities of pure MeOH [19] and its electrolyte solutions, respectively. A cut-off radius equal to half the box length was applied to all the interactions. Table 2 summarizes the designation, parameters, and some simulation details of the modelled systems.

The equations of motion were integrated with a time step of 1 fs by using an algorithm proposed and developed recently [20]. The MD simulations on all the systems were performed in the NVT ensemble by using the MDNAES simulation package [21]. The temperature was kept constant using the weak coupling method [22] with a relaxation time of 0.1 ps during collection runs of the already equilibrated systems. Equilibration periods of 100 ps and collection runs of 500 ps were used.

Table 3. The potential parameters for the interacting sites of the methanol molecule and ions.

Particle	Site[a]	σ_{ii} (Å)	ε_{ij} (kJ mol^{-1})	z_i (e)	M_i (amu)
MeOH	H_O	0.0	0.0	+0.431	1.007 947
	O	3.083	0.731 17	−0.728	15.999 43
	C (Me)	3.861	0.757 86	+0.297	15.034 941
Ni^{2+}	Ni^{2+}	0.85	615	+2	58.693 4
Cl^-	Cl^-	4.767	0.078 17	−1	35.452 7

[a] H_O refers to the hydroxyl hydrogen, and C (Me) refers to the methyl group treated as a united atom.

The site–site interactions between pairs of MeOH molecules and ions, as well as between a molecule and an ion are given by the sum of Lennard-Jones (LJ) 12-6 and Coulomb potentials,

$$U(r_{ij}) = 4\varepsilon_{ij}\left[\left(\frac{\sigma_{ij}}{r_{ij}}\right)^{12} - \left(\frac{\sigma_{ij}}{r_{ij}}\right)^{6}\right] + \frac{z_i z_j e^2}{4\pi\varepsilon_0 r_{ij}}, \tag{6}$$

where ε_{ij} and σ_{ij} are the LJ parameters between sites i and j of distinct molecules, z_i is the partial charge on site i, and r is the site–site separation. Cross interactions were obtained from Lorentz–Berthelot combining rules, $\varepsilon_{ij} = \sqrt{\varepsilon_{ii}\varepsilon_{jj}}$ and $\sigma_{ij} = (\sigma_{ii} + \sigma_{jj})/2$ [23]. A shifted force potential [21] was employed for the LJ part of the potential, whereas the reaction field method [24] was used to calculate the long-range Coulombic part.

The force field model of MeOH parameterized by Haughney *et al* [25], denoted as H1, and successfully used in our previous simulations [26], was used in the present MD simulations. Within the H1 model, each methanol molecule was treated as a rigid, non-polarizable object consisting of three sites corresponding to the oxygen (O), the methyl group (C) treated as a united atom, and the hydrogen of the hydroxyl group (H_O). The molecular geometry of the methanol molecule was described by two bond lengths, $d_{OHO} = 0.9451$ Å and $d_{CO} = 1.4246$ Å, and one angle $\angle COH_O = 108.53°$.

The LJ parameters for Cl^- were derived by fitting the LJ 12-6 potential function (first term on the right-hand side of equation (6)) to the van der Waals curve calculated by the equation

$$U^{vdW}(r_{ii}) = \varepsilon_{ii}^{vdW}\left[2\left(\frac{R_{ii}^*}{r_{ii}}\right)^9 - 3\left(\frac{R_{ii}^*}{r_{ii}}\right)^6\right], \tag{7}$$

in the range 3.5–7.0 Å by using ε_{ii}^{vdW} and R_{ii}^* parameters proposed by Peng *et al* [27].

The LJ parameters, ε_{NiNi} and σ_{NiNi}, for the nickel cation were obtained in the following way. First, the LJ parameters ε_{NiO} and σ_{NiO} were derived by fitting the LJ 12-6 potential function (first term in the right-hand part of equation (6)) to the potential curve describing an interaction of Ni^{2+} with a six-site water molecule [28]. Then, the LJ parameters ε_{NiNi} and σ_{NiNi} were calculated by using the SPC/E model for water [29] and Lorentz–Berthelot combining rules. We consider such a procedure as quite reasonable because, both within the SPC/E model for water and H1 model for methanol, the hydroxyl hydrogen is considered similarly as a charged site with zero LJ parameters. All the potential parameters used in the present MD simulations are listed in table 3.

5. MD simulations results and their discussion

5.1. Structure and force field model validation

The structural properties of the solutions have been characterized by a set of radial distribution functions (RDFs), $g_{\alpha\beta}(r)$, together with the running co-ordination numbers (r.c.ns), $n_{\alpha\beta}(r)$,

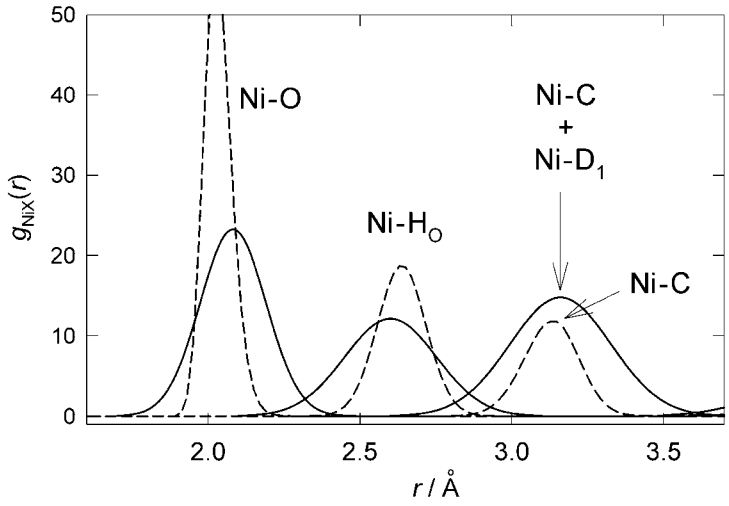

Figure 7. The RDFs, $g_{\mathrm{NiX}}(r)$ (full curves), describing the nearest-neighbour environment of Ni^{2+} in ∼1.4 molal $NiCl_2$–methanol solutions as obtained by using NDIS technique. The dashed curves are the same RDFs derived from MD simulation on system VI (see table 2).

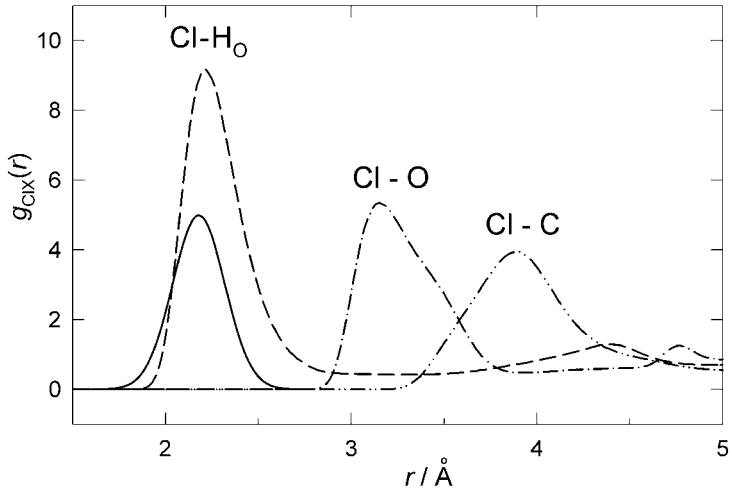

Figure 8. The RDF, $g_{\mathrm{ClH_O}}(r)$ (full curve), as obtained by using the NDIS technique on ∼1.4 molal $NiCl_2$–methanol solution. All other curves are the RDFs, $g_{\mathrm{ClX}}(r)$, describing the nearest-neighbour environment of Cl^- derived from MD simulations on system VI (see table 2).

defined as

$$n_{\alpha\beta}(r) = 4\pi\rho_\beta \int_0^r g_{\alpha\beta}(r')r'^2\,\mathrm{d}r', \tag{8}$$

where ρ_β is the number density of species β. The ion–solvent RDFs, $g_{\mathrm{iX}}(r)$, between the ion i (Ni^{2+} and Cl^-) and X (X = H_O/O/C) site of the MeOH molecule, as well as Ni–Cl and Cl–Cl RDFs derived from MD simulation on systems V and VI are displayed in figures 7–9. The experimental RDFs obtained by using the neutron diffraction with isotopic substitution (NDIS) technique on ∼1.4 molal $NiCl_2$–MeOH solutions [14, 15] are also plotted in these figures. The positions of the first maxima in the RDFs for systems III–VI along with the experimental

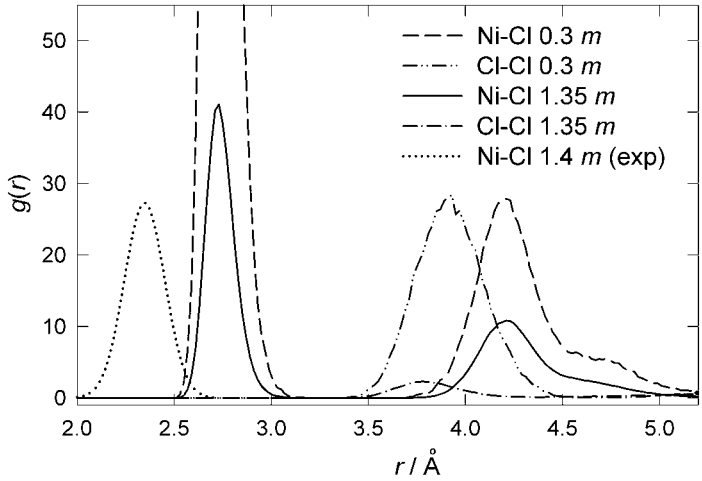

Figure 9. The RDFs, $g_{\mathrm{NiCl}}(r)$ and $g_{\mathrm{ClCl}}(r)$, derived from MD simulations on systems V (dashed and double dot–dashed curves, respectively) and VI (solid and dot–dashed curves, respectively) corresponding to ∼0.3 and ∼1.35 molal solutions of $NiCl_2$ in MeOH (see table 2). The dotted curve corresponds to the experimental RDF, $g_{\mathrm{NiCl}}(r)$, obtained by using the NDIS technique on ∼1.4 molal solution of $NiCl_2$ in MeOH.

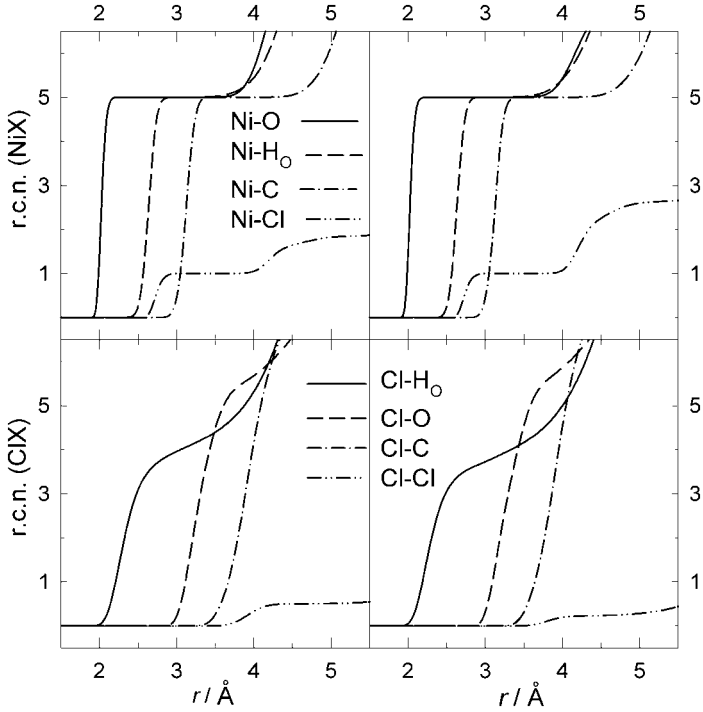

Figure 10. The running co-ordination numbers of Ni^{2+} and Cl^- ions in ∼0.3 molal (left) and ∼1.35 molal (right) solutions of $NiCl_2$ in MeOH at 298 K derived from MD simulations on systems V and VI (see table 2), respectively.

values are listed in table 4. The corresponding running co-ordination numbers for the ∼0.3 and ∼1.35 molal solutions are shown in figure 10.

Table 4. The positions of the first maxima in the RDFs for ion–X (X = the closest atom of the MeOH molecule) and ion–ion pairs from MD simulations on systems III–VI (also see figures 7–9 for systems V and VI) and NDIS experiments on ∼1.35 molal solutions of $NiCl_2$ in methanol. (Note: the positions of the second maxima are given in parentheses. The positions of the first minima are indicated only for the pairs used for defining the boundaries of the first solvation shells of the ions.)

		$r_{max\,1}$ (Å)	$r_{min\,1}$ (Å)	$r_{max\,1}$ (Å)
System	Pairs	MD simulations		NDIS experiments[a,b]
III	Ni^{2+}–O	2.03	3.0	—
III	Ni^{2+}–H_O	2.64	—	—
III	Ni^{2+}–C	3.14	—	—
IV	Cl^-–H_O	2.28	3.27	—
IV	Cl^-–O	3.19	—	—
IV	Cl^-–C	3.89	—	—
V	Ni^{2+}–O	2.03	2.8	—
V	Ni^{2+}–H_O	2.64	—	—
V	Ni^{2+}–C	3.13	—	—
V	Ni^{2+}–Cl^-	2.72 (4.21)	—	—
V	Cl^-–H_O	2.25	3.25	—
V	Cl^-–O	3.19	—	—
V	Cl^-–C	3.88	—	—
V	Cl^-–Cl^-	3.92	—	—
VI	Ni^{2+}–O	2.03	2.5	2.057
VI	Ni^{2+}–H_O	2.64	—	2.619
VI	Ni^{2+}–C	3.13	—	3.163
VI	Ni^{2+}–Cl^-	2.72 (4.21)	—	2.348
VI	Cl^-–H_O	2.21	3.0	2.18
VI	Cl^-–O	3.15	—	3.077–3.215
VI	Cl^-–C	3.88	—	3.632–3.810
VI	Cl^-–Cl^-	3.78	—	4.57[c]

[a] Reference [14].
[b] Reference [15].
[c] This value can be considered merely indicative because it was obtained from a rather noisy high-order difference function (see figure 6 in [15]).

The Ni^{2+}–$O/H_O/C$ (MeOH) and Ni–Cl RDFs show (figures 7, 9) intense first peaks, especially for the cation–O and cation–Cl pairs in the solutions of both concentrations. These clearly indicate the formation of well-defined first co-ordination shells around Ni^{2+}. The RDFs of the pairs with the Cl^- ion also show (figures 8, 9) well-defined first peaks, but these are of reduced intensities, broader, and their first minima are much shallower as compared to those for the nickel. These observations are clear testimony to a more crumbly packing of the MeOH molecules around the anion as compared with the cation.

The change in the concentration of $NiCl_2$–MeOH solution appears to hardly influence the ion–$O/H_O/C$ (MeOH) RDFs, and this is also reflected in the corresponding running coordination numbers (figure 10). Only small shifts in the positions of the first peaks towards shorter distances with increase in electrolyte concentration can be observed (see table 4) for the Cl^- ion.

Comparison of the MD simulated RDFs with the corresponding ones obtained from NDIS experiments [14, 15] shows (figures 7, 8 and table 4) a good agreement in the first peak positions for Ni–O, Ni–H_O, Ni–C, Cl–H_O, Cl–O, and Cl–C pairs. Although the first peaks in the simulated RDFs $g_{NiX}(r)$, describing the nearest-neighbour environment of Ni^{2+} in ∼1.35 molal

$NiCl_2$–methanol solutions, are narrower than the experimental ones (figure 7), figure 10 unambiguously indicates the stability of the cation's first co-ordination shell as composed of five MeOH molecules and one Cl^- ion. This is especially encouraging because these results are exactly the same as those obtained previously by us from the NDIS experiments [14]. The well-defined plateaus in the functions $n_{NiX}(r)$ in the range ∼2–4 Å (figure 10) confirm, once again, the stability of the first solvation shell of Ni^{2+}.

In contrast to the Ni^{2+} cation, evaluation of the anion (Cl^-) co-ordination (solvation) number through the integration procedure described by equation (8) is hampered because of a lack of a zero minimum after the first maximum in all the RDFs pertaining to Cl–X pairs (figure 8). As a result, the $n_{ClX}(r)$ functions for chloride show a monotonic increase with r (figure 10). Thus, the solvation number of the Cl^- ion depends on the definition of the FSS boundary and can be estimated from the $n_{ClH_O}(r)$ to be in the range 3.5–4.5. This value is slightly more than 1.6–2.9, the value derived by using second- and higher-order isotopic difference techniques of neutron diffraction (tables 5 and 6 in [15]).

The first peak at 2.72 Å in the computed Ni–Cl RDF for ∼1.35 molal solution occurs at slightly larger inter-ion distance as compared with the one obtained at 2.35 Å from NDIS experiments (figure 9, table 4). Probably, this difference arises from the fact that Ni–Cl pair potential expressed by equation (7) was not specially adjusted for this interaction to incorporate a possible covalent contribution typical for a d-block element like Ni. Nevertheless, the force field models (table 3) employed in this work allowed us not only to reproduce correctly the experimental co-ordination number of Ni^{2+} with respect to Cl^- equal to unity [15] (see figure 10), but also to confirm the Cl–Cl short-range correlation [2] occurring around 4 Å (figure 9). The latter observation corroborates our earlier findings [15] about the existence of solvated ion triples $[NiCl_2]_s^+$ in concentrated solutions of $NiCl_2$ in methanol.

Overall, the comparison of structural properties of ∼1.35 molal solution of $NiCl_2$ in MeOH obtained from MD simulations and NDIS experiments indicates the reliability of force field models employed in our MD modelling. A deeper molecular insight of the microscopic structure of $NiCl_2$–MeOH solutions, inaccessible from real experiments, can thus be gained from the current MD simulations.

The results reported in figure 9 and table 4 allow us to identify the presence of not only the contact ion pair (CIP) $[NiCl]^+$ at an inter-ionic distance of 2.72 Å, but also the solvent separated ion pair (SSIP) at 4.21 Å. It is interesting to note that a change in electrolyte concentration from ∼0.3 to ∼1.35 molal does not influence the inter-ionic distances in these ionic aggregates. It is also noteworthy that the existence of SSIPs could not be revealed from the NDIS experiments, probably due to a relatively small contribution from Ni–Cl correlation to the experimental signal (see table 3 and figure 16 in [14]).

For further microscopic considerations of ion solvation phenomenon, the distributions of co-ordination numbers (c.ns) within the first solvation shells of the ions, n_1, constructed by direct counting [12], were analysed (figure 11). The averaged co-ordination (solvation) numbers over the first solvation shells, $n_{1,av}$, of Cl^- derived from the corresponding distributions are also listed in figure 11. The definition of the FSS boundary in each of the modelled systems III–VI was based on the position of the first minimum (see table 4) in the Ni^{2+}–O and/or Cl^-–H_O RDFs.

In the infinitely dilute solution of Ni^{2+} in MeOH (system III), the probability distribution function is uni-modal, with the most probable value being exactly equal to 6. In the solutions of finite concentrations, however, the average c.n. of the cation decreases to 5 due to ion association. It is interesting to note that in ∼1.35 molal solution, the values of 4 and 6 for nickel co-ordination (solvation) by MeOH molecules are also possible with a high probability (figure 11, left). For a visual interpretation of the corresponding distributions, the snapshots

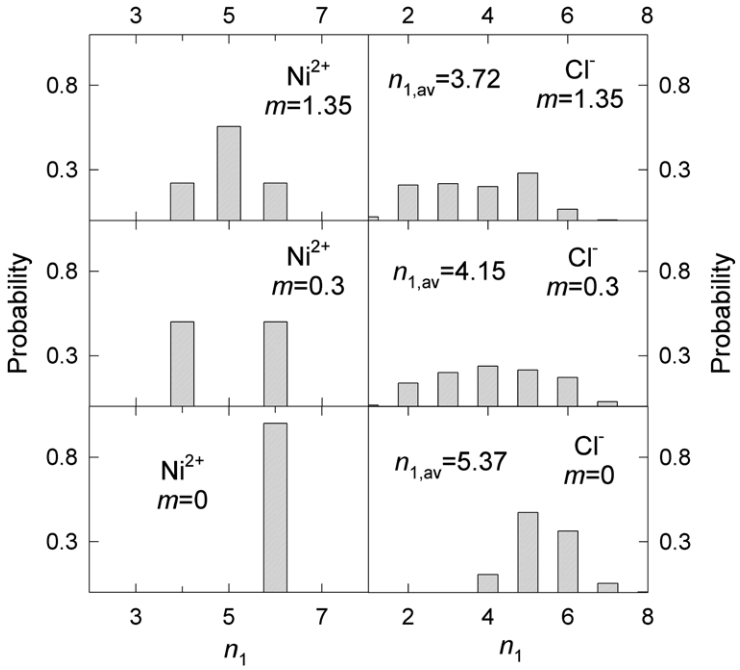

Figure 11. The distribution of co-ordination numbers (c.ns) of Ni^{2+} (left) and Cl^{-} (right) in their first solvation shells from MD simulations at 298 K of systems III (bottom left), IV (bottom right), V (middle), and VI (top) (for the system definitions see table 2).

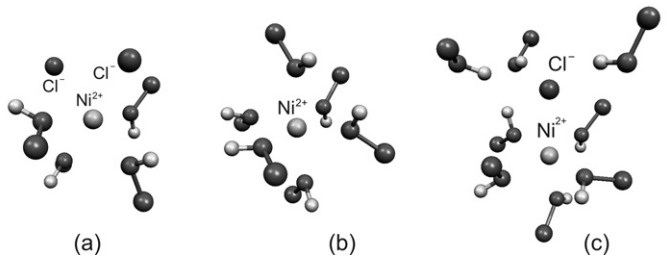

Figure 12. Instantaneous configurations of co-ordination shells of Ni^{2+} in 1.35 molal solution of $NiCl_2$ in MeOH at 298 K (from MD simulations) with c.n. $= 4 + 2$ (a), c.n. $= 6 + 0$ (b), and c.n. $= 5 + 1$ (c). In figure (c) the configuration of the solvation environment of $[NiCl]^{+}$ contact ion pair can also be seen.

of the instantaneous configurations of co-ordination shells of Ni^{2+} in ∼1.35 molal solution of $NiCl_2$ in MeOH at 298 K are shown in figure 12. Figure 12(a) suggests that for a possible co-ordination shell of Ni^{2+}, comprising four MeOH molecules and two chloride ions, the latter (Cl^{-}) lie on an edge of the octahedron and not in the radial positions, as one would expect. Surprisingly, the mean co-ordination number of Ni^{2+} in the ∼0.3 molal solution is still 5, but it results from equal contributions from the 4 and 6 c.n. values. Thus, the solvation number 5 is not stable in dilute solutions of $NiCl_2$ in methanol. Clearly, the results described above cannot be deduced from any diffraction experiment due, in principle, to the time (for data collection) and space (throughout the macroscopic volume of the solution) averaging nature of the structural data so derived.

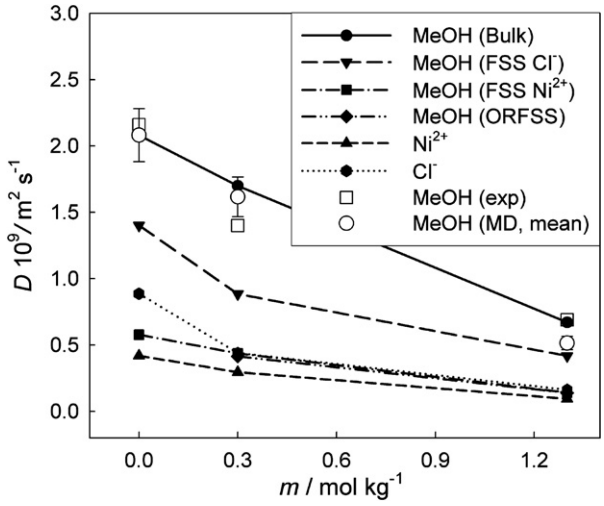

Figure 13. Simulated and/or experimental translational diffusion coefficients, D, of Ni^{2+}, Cl^-, and MeOH molecules belonging to the bulk solvent, the first solvation shells (FSSs), and the region of overlap of the ions' FSSs (ORFSS) in $NiCl_2$–MeOH solutions at 298 K as a function of the solution's molality. The simulated diffusion coefficients of methanol molecules related to the whole electrolyte solutions (MD, mean) are also presented.

As opposed to the cation, rather wide distributions of n_1 are observed (figure 11, right) for Cl^-, with the mean, $n_{1,\mathrm{av}}$, value decreasing from 5.37 for infinitely dilute solution ($m \Rightarrow 0$ mol kg^{-1}) to 3.72 for a concentrated solution ($m = \sim 1.35$ mol kg^{-1}). This is quite reasonable because the behaviour of the corresponding RDFs (figures 7, 8) is different in regions of the first minima. The function $g_{\mathrm{NiO}}(r)$ shows a very sharp first peak followed by a zero-value minimum, whereas the Cl–H_O RDF does not have a zero value around the first minimum.

5.2. Translational diffusion of methanol molecules

Self-diffusion coefficients, D, of the centre of mass of MeOH molecules and ions were calculated from the mean-absolute displacements (MADs),

$$\lim_{t\to\infty} R_1(t) = \lim_{t\to\infty} \langle |\mathbf{r}(t) - \mathbf{r}(0)| \rangle = 4(Dt/\pi)^{1/2}, \tag{9}$$

the mean-square displacements (MSDs),

$$\lim_{t\to\infty} R_2(t) = \lim_{t\to\infty} \langle |\mathbf{r}(t) - \mathbf{r}(0)|^2 \rangle = 6Dt, \tag{10}$$

and the velocity autocorrelation functions (VACFs) via the Green–Kubo relation,

$$D = \lim_{t\to\infty} \tfrac{1}{3} \int_0^\infty \langle \mathbf{v}(0)\mathbf{v}(t) \rangle \, \mathrm{d}t. \tag{11}$$

In order to investigate how the presence of Ni^{2+} and Cl^- ions influence the dynamical behaviour of the solvent molecules throughout the electrolyte solution, the diffusion coefficients of MeOH molecules have been calculated separately in different regions (methanol subsystems)—the bulk solvent (Bulk), the first (FSS) and second (SSS) solvation shells of ions, and the overlapping region of the first solvation shells (ORFSS) of Ni^{2+} and Cl^-. The resulting D_{MeOH} and D_i values for all the simulated systems are summarized in table 5 and shown in figure 13. Figure 13 also depicts the experimental and simulated 'overall' diffusion coefficients,

Table 5. Self-diffusion coefficients of the methanol molecules and ions in the modelled systems (see table 2), derived from the centre of mass of the velocity autocorrelation functions (VACFs), mean absolute displacements (MADs), and mean-square displacements (MSDs). Bulk, FSS, SSS, and ORFSS stand for the bulk solvent, the first and second solvation shells of an ion, and the overlapping region of the fist solvation shells of Ni^{2+} and Cl^-, respectively.

		D (10^5 cm^2 s^{-1})				
System	Particle/Region	VACF	MAD	MSD	Mean	Residence time (ps)
I	MeOH/Bulk	0.27	0.26	0.28	0.27	—
II	MeOH/Bulk	2.03	1.99	2.03	2.0	—
III	MeOH/Bulk	2.08	2.06	2.10	2.1	—
III	MeOH/SSS Ni^{2+}	1.17	0.87	0.93	1.0	94
III	MeOH/FSS Ni^{2+}	0.57	0.57	0.59	0.58	>500[a]
III	Ni^{2+}	0.41	0.42	0.43	0.42	—
IV	MeOH/Bulk	2.01	1.99	2.03	2.0	—
IV	MeOH/SSS Cl^-	1.77	2.45	2.50	2.2	17
IV	MeOH/FSS Cl^-	1.53	1.31	1.36	1.4	50
IV	Cl^-	0.92	0.86	0.87	0.89	—
V	MeOH/Bulk	1.72	1.66	1.72	1.7	—
V	MeOH/FSS Cl^-	1.01	0.81	0.84	0.88	61
V	MeOH/FSS Ni^{2+}	0.47	0.41	0.43	0.44	227
V	MeOH/ORFSS	0.42	0.40	0.41	0.41	147
V	Ni^{2+}	0.30	0.29	0.29	0.29	—
V	Cl^-	0.45	0.43	0.43	0.44	—
VI	MeOH/Bulk	0.70	0.61	0.69	0.67	—
VI	MeOH/FSS Cl^-	0.60	0.31	0.34	0.42	52
VI	MeOH/FSS Ni^{2+}	0.13	0.14	0.15	0.14	143
VI	MeOH/ORFSS	0.14	0.13	0.14	0.14	86
VI	Ni^{2+}	0.096	0.091	0.096	0.094	—
VI	Cl^-	0.16	0.16	0.17	0.16	—

[a] During the collection run of 500 ps, no decay in residence time correlation function (RTCF) of MeOH molecules for this subsystem was observed (see figure 14(a)).

denoted as 'exp' and 'MD, mean', respectively, of methanol molecules related to the whole electrolyte solutions at three different concentrations ($m \Rightarrow 0, 0.3$, and 1.35 mol kg^{-1}). The following conclusions can be drawn from analysis of the data listed in table 5 and shown in figure 13.

(1) The diffusion coefficients estimated by different means, e.g., from the VACF, MAD, and MSD, are in reasonable agreement (see table 5) with each other.
(2) The experimental D_{MeOH} values derived from the QENS experiments are in satisfactory agreement (see figure 13) with the 'overall' simulated diffusion coefficients averaged throughout each solution by taking into account the molar fractions of the solvent molecules in different subsystems (regions).
(3) Due to the relatively small fraction of MeOH molecules in the first solvation shells of the ions as compared to the total number of solvent molecules, the 'overall' simulated average values of D_{MeOH} differ only slightly (see figure 13) from those in the bulk solvent. Because of this, it is difficult to extract the diffusion coefficients of the MeOH molecules within an ion's FSS from the real physical experiment.
(4) In the electrolyte solution of a finite concentration (0.3 m—system V), the values for the diffusion coefficients of Cl^- and MeOH molecules from Ni^{2+} FSS and ORFSS are close among themselves, and these values are approximately four times smaller than the D_{MeOH}

in the bulk. Similarly, in the infinitely dilute solution of Ni^{2+} (system III), the diffusion coefficient of MeOH molecules from Ni^{2+} FSS is ∼4 times smaller than the corresponding D_{MeOH} in the bulk. These observations indicate that the translational diffusion of the nearest neighbouring environment of Ni^{2+} is fully controlled by the strong interactions of the cation with its immediate environment.

(5) As the concentration of electrolyte increases or, in other words, as the molar ratio of solvent to solute decreases from 215:1 (system III) to 21:1 (system VI), the D_{MeOH} values decrease substantially not only in the FSS of Ni^{2+} but also in the bulk. This shows that the translational diffusion motion of methanol molecules slows down drastically both in the Ni^{2+} FSS and in the bulk. This can be the result of drawing the whole electrolyte system into the strong electrostatic field created by the ion subsystem at higher electrolyte concentrations.

(6) In contrast to Ni^{2+}, the influence of Cl^- on the translational diffusion of methanol molecules is restricted by only its FSS. It is interesting to note that for all the simulated systems, the ratios of diffusion coefficients of MeOH molecules from Cl^- FSS and those of Cl^- itself remain practically constant within 2.1 ± 0.5.

It emerges from the above discussion that the dynamic properties of all the MeOH molecules in its electrolyte solution are influenced by both the cation and anion, and are expected to differ from pure methanol significantly, especially at high concentrations of the electrolyte.

Having shown that the pair potentials employed in the simulations lead to good agreement between the simulated and experimental results, it can be reasonably expected that the properties which are not directly accessible by the experiments can be calculated from the simulations with a high degree of reliability.

To further examine the dynamic properties of all the MeOH molecules around the ions, we evaluated the residence time correlation functions, RTCFs, of the solvent molecules in the solvation shells. The RTCF yields an estimate of 'life time' of the solvent molecules near an ion, and this can be compared with the 'binding time' widely used in the theory of QENS. The RTCFs have been calculated as [30]

$$\mathrm{RTCF}(t) = \frac{1}{n_\alpha} \sum_{i=1}^{n_\alpha} \langle \theta_\alpha(r, 0)\theta_\alpha(r, t)\rangle, \tag{12}$$

where $\theta_\alpha(r, t)$ is the Heaviside unit step-function that is 1 if a methanol molecule i is in region r within a co-ordination shell α of the ion, and 0 otherwise. n_α is the average number of methanol molecules in the co-ordination shell α at $t = 0$.

The RTCFs as a function of time are displayed in figure 14 for the MeOH molecules in the simulated systems III–VI. Clearly, these correlation functions can be reasonably described by an exponential decay. The residence times of the solvent molecules in the solvation shells of Ni^{2+} and Cl^-, as obtained by fitting the RTCFs to exponential decay functions, are included in table 5.

Since the D_{MeOH} value in the second solvation shell of Cl^- in its infinitely dilute solution (system IV) is found to be quite similar to that in the bulk solvent (table 5), one can consider the residence time (17 ps) of MeOH molecules in this region simply as an estimate of the residence time also in the bulk. Starting from this basis, the residence times of MeOH molecules in the FSS of Ni^{2+} are found to be at least one order of magnitude more as compared with those in the bulk solvent in infinitely dilute solutions.

It is interesting to note that the residence time of MeOH molecules in the FSS of Ni^{2+} decrease significantly with increase in the electrolyte concentration, whereas the corresponding values in the FSSs of Cl^- remain practically unchanged within ∼50–60 ps. This result is

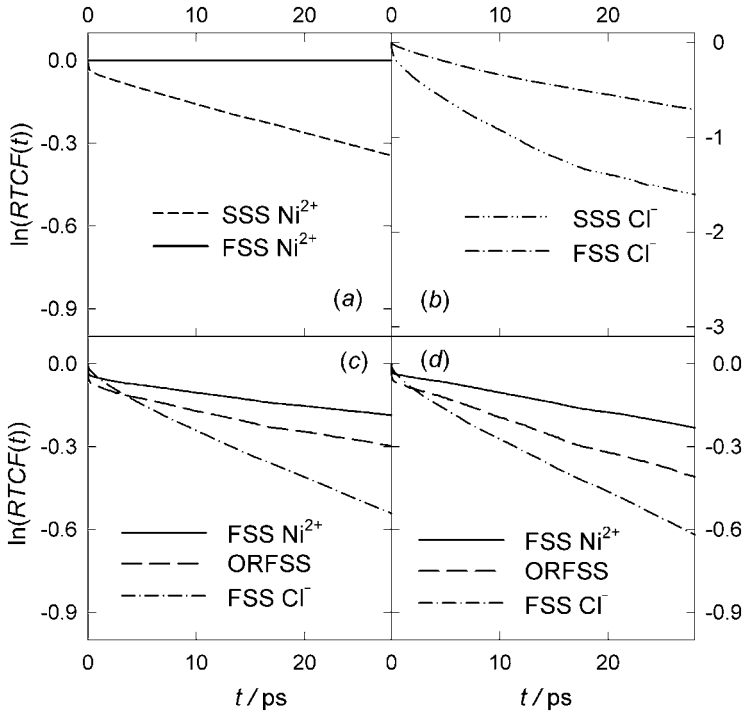

Figure 14. Residence time correlation functions (RTCFs) for the methanol molecules in the first (FSS) and second (SSS) solvation shells of ions, and in the overlapping region of the cation's and anion's first solvation shells (ORFSS) as derived from the MD simulations on systems III (a), IV (b), V (c), and VI (d) (for system's definition see table 2).

consistent with the observed tendency (see figure 11) in the change of c.n. distributions within the FSSs of Ni^{2+} and Cl^{-}. This may be explained partly in terms of higher sensitivity of the cation's FSS to mutual inter-ion interactions, resulting from the anion's penetration into the cation's FSS, especially in electrolyte solutions of finite concentrations.

5.3. Hindered translations and librations of methanol molecules

The spectral densities of the hindered translational, $S_{\mathbf{vv}}(\omega)$, and librational, $S_{\mathbf{ww}}(\omega)$, motions of MeOH molecules have been calculated by the cosine Fourier transformation,

$$S_{\mathbf{AA}}(\omega) = \int_0^\infty C_{\mathbf{AA}}(t)\cos(\omega t)\,\mathrm{d}t, \tag{13}$$

of the corresponding normalized velocity autocorrelation functions (VACFs) of translational, $C_{\mathbf{vv}}(t)$, and rotational, $C_{\mathbf{ww}}(t)$, motion of the methanol molecules,

$$C_{\mathbf{AA}}(t) = \langle \mathbf{A}(0)\mathbf{A}(t)\rangle / \langle \mathbf{A}(0)\mathbf{A}(0)\rangle, \tag{14}$$

where $\mathbf{A} \equiv \mathbf{v}$ or $\mathbf{w}$. The results are presented in figures 15–17.

The distinct feature of the rotational VACFs, $C_{\mathbf{ww}}(t)$, is their oscillatory behaviour, which is present not only in the ions' FSSs, but also in the bulk solvent. This implies that the rotational motion of methanol molecules in electrolyte solutions is restricted by their strong interactions either with ions or due to H-bonding with the nearest solvent molecules.

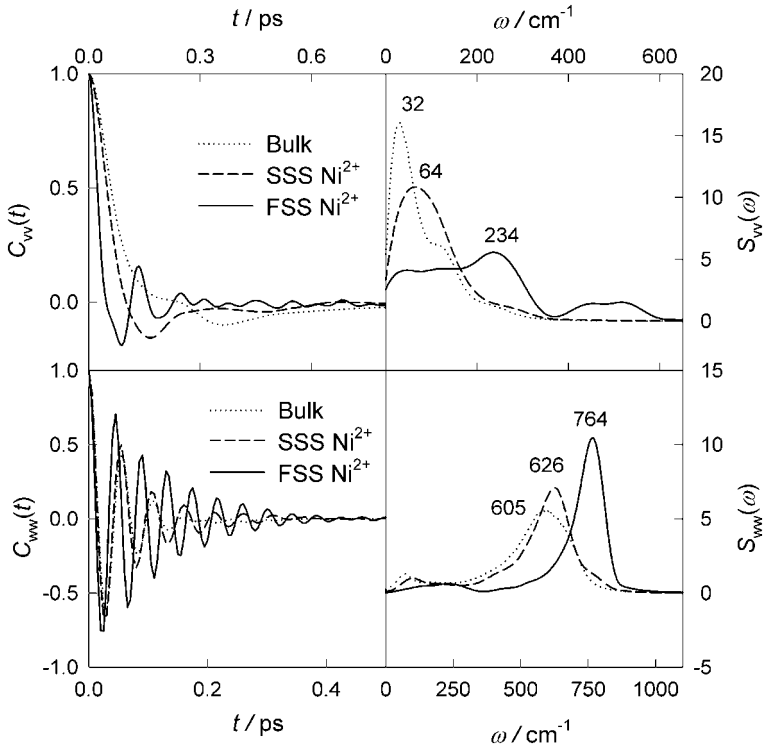

Figure 15. Normalized autocorrelation functions (ACFs) of the translational [$C_{\mathbf{vv}}(t)$] and rotational [$C_{\mathbf{ww}}(t)$] motions of the methanol molecules in the bulk solvent (Bulk), the first (FSS) and the second (SSS) solvation shells of Ni^{2+} in the system III (see table 2). $S_{\mathbf{vv}}(\omega)$ and $S_{\mathbf{ww}}(\omega)$ (on the right) are cosine Fourier transforms of the corresponding ACFs (on the left), and represent the spectral densities of the hindered translation and libration motions of the MeOH molecules.

The influence of Ni^{2+} on the MeOH molecules in its (Ni^{2+}) FSS is observed in the blue shifts. The frequency of hindering translation and libration of methanol molecules in the FSS of Ni^{2+} are shifted by ∼150–210 cm^{-1} with respect to the bulk solvent for both the hindered translation and libration. The influence of Cl^- on the spectral density functions, $S_{\mathbf{vv}}(\omega)$ and $S_{\mathbf{ww}}(\omega)$, of MeOH molecules in its FSS is small relative to that of Ni^{2+}, and the frequency values are comparable to that in the SSS of Ni^{2+} in the infinitely dilute solution. Interestingly, however, the dynamic behaviour of MeOH molecules in the ORFSS in solutions of finite concentrations is quite similar to that in the FSS of the cation.

6. Conclusions

The high-resolution quasi-elastic neutron scattering (QENS) technique has been applied to study the translational diffusion of methanol protons in pure methanol (MeOH) at 223 and 297 K, and in 0.3 and 1.3 molal solutions of $NiCl_2$ in methanol at 297 K. Molecular dynamics (MD) simulations have also been carried out in the NVT ensemble to explore the static and dynamic behaviour of the experimentally investigated systems. The MD simulated results validate our structural results at the pair distribution function level obtained previously by neutron diffraction isotopic substitution (NDIS) technique.

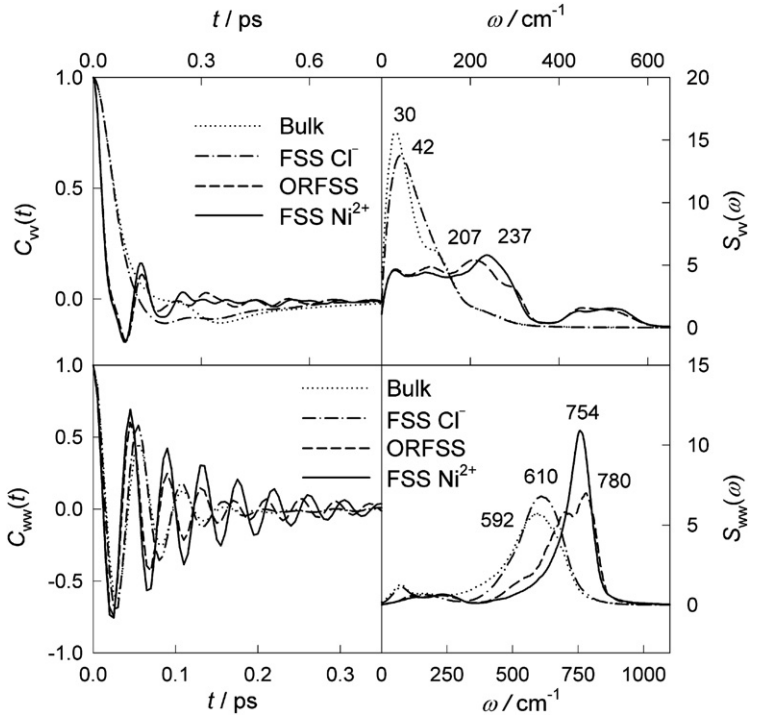

Figure 16. Normalized autocorrelation functions (ACFs) of translational [$C_{\mathbf{vv}}(t)$] and rotational [$C_{\mathbf{ww}}(t)$] motion of the methanol molecules in the bulk solvent (Bulk), the first solvation shells (FSS), and the overlapping region of the cation's and anion's first solvation shells (ORFSSs) in the system V (see table 2). $S_{\mathbf{vv}}(\omega)$ and $S_{\mathbf{ww}}(\omega)$ (on the right) are the cosine Fourier transforms of the corresponding ACFs (on the left), and represent the spectral densities of the hindered translation and libration motion of the MeOH molecules.

The translational diffusion coefficients (D) derived from the QENS measurements of pure methanol at the two temperatures and of the two solutions of nickel chloride in methanol at different concentrations agree well with the values reported in the literature. These results clearly indicate that the diffusion coefficient of methanol decreases (i) with decrease in temperature in pure methanol, and (ii) with increase in the concentration of $NiCl_2$ in methanol. The present MD simulations confirm the above experimental findings.

The MD results show that it is mainly the solvent molecules present in the bulk that govern the dynamic behaviour of methanol molecules in its electrolyte solutions. The diffusion coefficients of the Ni^{2+}, of MeOH molecules in the first solvation shell (FSS) of Ni^{2+}, and also of its counter-ion, the Cl^{-}, are very close to each other and follow similar trends with the change in the concentration of the electrolyte. These observations are a clear testimony to the high stability of the complex formed by nickel ion with the solvent molecules and its counter-ion.

The dynamic stability of the $[Ni(MeOH)_5Cl]^{+}$ complex revealed by the present MD simulations cannot be observed directly from the QENS experiments. The QENS results reveal only the values of D, averaged over the whole solution, and do not provide any microscopic details.

Analysis of the molecule dynamics in terms of diffusion coefficients and autocorrelation functions of angular and centre-of-mass velocities, and unit vectors of dipole moment and main

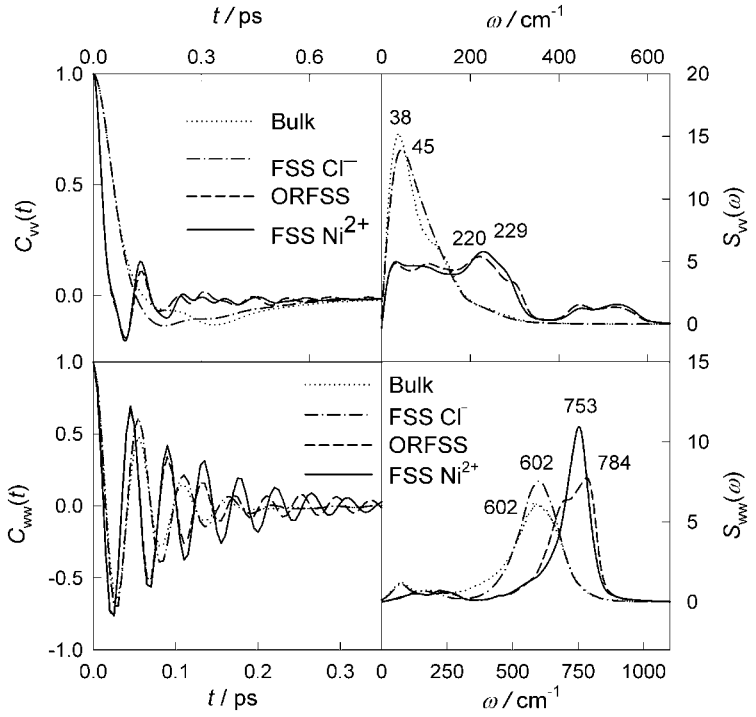

Figure 17. Normalized autocorrelation functions (ACFs) of translational [$C_{\mathbf{vv}}(t)$] and rotational [$C_{\mathbf{ww}}(t)$] motion of the methanol molecules in the bulk solvent (Bulk), the first solvation shells (FSS), and the overlapping region of the cation's and anion's first solvation shells (ORFSSs) in the system VI (see table 2). $S_{\mathbf{vv}}(\omega)$ and $S_{\mathbf{ww}}(\omega)$ (on the right) are cosine Fourier transforms of the corresponding ACFs (on the left), and represent the spectral densities of the hindered translation and libration motion of the MeOH molecules.

inertia axes show that a cation of small size and high charge, such as Ni^{2+}, forms a dynamically well-defined solvation shell. Also, with decrease in the ion–molecule distance, the mobility of solvent molecules decreases significantly for such ions of high charge density.

Acknowledgments

AKA, is grateful to the Institute Laue Langevin (ILL, Grenoble) for allocation of neutron beam time, Dr M R Johnson (ILL) for help with the QENS experiments, and the University of Abertay Dundee (UAD), UK, for support of his research activities. ONK thanks the Kharkiv National University, Ukraine, for providing him the necessary resources, and the UAD for hosting his visits. AKA gratefully acknowledges the financial support received from the Carnegie Trust (UK), and the Royal Society of Edinburgh (UK) to enable mutual exchange of visits between the collaborating partners from Ukraine (ONK) and the UK (AKA).

References

[1] Frank H S and Wen W-Y 1957 *Discuss. Faraday Soc.* **24** 133
[2] Neilson G W and Enderby J E 1996 *J. Phys. Chem.* **100** 1317
[3] Neilson G W and Adya A K 1997 *Annu. Rep. C: Royal Soc. Chem.* **93** 101

[4] Adya A K 2002 *Molten Salts from Fundamentals to Applications* ed M Gaune-Escard (Dordrecht: Kluwer) p 107
[5] Neilson G W, Adya A K and Ansell S 2002 *Annu. Rep. C: Royal Soc. Chem.* **98** 273
[6] Adya A K 2005 *J. Ind. Chem. Soc.* **82** 1197
[7] Hewish N A, Enderby J E and Howells W S 1983 *J. Phys. C: Solid State Phys.* **16** 1777
[8] Kunz W, Calmettes P and Bellissent-Funel M-C 1993 *J. Chem. Phys.* **99** 2079
[9] Salmon P S 1987 *J. Phys. C: Solid State Phys.* **20** 1573
[10] Novikov A G, Rodnikova M N, Savostin V V and Sobolev O V 1997 *Physica* B **234–236** 340
[11] Bermejo F J, Batallan F, Enciso E, White R, Dianoux A J and Howells W S 1990 *J. Phys.: Condens. Matter* **2** 1301
[12] Adya A K, Kalugin O N, Volobuev M N and Kolesnik Ya V 2001 *Mol. Phys.* **99** 835
[13] Kalugin O N, Adya A K, Volobuev M N and Kolesnik Ya V 2003 *Phys. Chem. Chem. Phys.* **5** 1536
[14] Kalugin O N and Adya A K 2000 *Phys. Chem. Chem. Phys.* **2** 11
[15] Adya A K and Kalugin O N 2000 *J. Chem. Phys.* **113** 4740
[16] Karyakin Yu V and Angelov I U 1974 *Pure Chemical Substances* (Moscow: Khimiya Publishers)
[17] Pratt K C and Wakeham W A 1977 *J. Chem. Soc. Faraday Trans.* II **73** 997
[18] Sampson T E and Carpenter J M 1969 *J. Chem. Phys.* **51** 5543
[19] Barthel J, Wachter R and Gores H-J 1979 *Modern Aspects of Electrochemistry* vol 13, ed B E Conway and J O'M Bockis (New York: Plenum) p 1
[20] Kolesnik Ya V, Kalugin O N and Volobuev M N 2001 *Khim. Fiz. (Russ.)* **20** 16
[21] Kalugin O N, Volobuev M N and Kolesnik Ya V 1999 *Kharkov Univ. Bull., Chem. Ser.* **454** 58
[22] Berendsen H J C, Postma J P M, van Gunsteren W, DiNola A and Haak J R 1984 *J. Chem. Phys.* **81** 3684
[23] Allen M P and Tildesley D J 1987 *Computer Simulation of Liquids* (Oxford: Clarendon)
[24] Neumann M 1985 *J. Chem. Phys.* **82** 5663
[25] Haughney M, Ferrario M and McDonald I R 1987 *J. Phys. Chem.* **91** 4934
[26] Bianchi L, Kalugin O N, Adya A K and Wormald C J 2000 *Mol. Simul.* **25** 321
[27] Peng Z, Ewig C S, Hwang M-J, Waldman M and Hagler A T 1997 *J. Phys. Chem.* A **101** 7243
[28] Odelius M, Ribbing K and Kowalewski J 1995 *J. Chem. Phys.* **103** 1800
[29] Berendsen M J C, Grigera J R and Straatsma T P 1987 *J. Phys. Chem.* **91** 6271
[30] Impey R W, Madden P A and McDonald I R 1985 *J. Chem. Phys.* **87** 5071